Seismic fragility assessment of integral precast multi-span bridges in areas of moderate seismicity
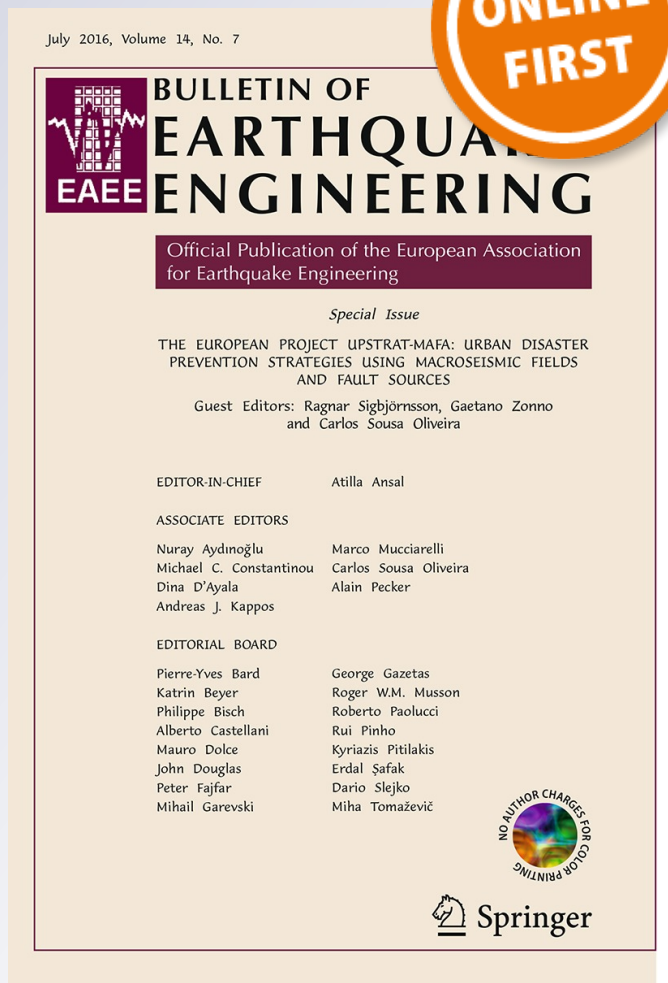
József Simon & László Gergely Vigh

ONLINE FIRST

Springer

CrossMark

ORIGINAL RESEARCH PAPER

Seismic fragility assessment of integral precast multi-span bridges in areas of moderate seismicity

József Simon[1] · **László Gergely Vigh**[1]

Abstract In lack of seismic provisions in the pre-Eurocode ages, most of the existing Hungarian bridges were not designed for seismic actions, therefore their seismic performance is questionable. The most commonly used structural type in highway construction is the integral precast multi-girder bridge. These bridges are typically constructed as continuous multi-support systems with monolithic joints at each support, thus their behavior may be significantly different from those applying simply supported beams and conventional bearings. A parametric fragility analysis of a wide range of different layouts is carried out using detailed and advanced non-linear numerical models. The results indicate that the abutment joints are highly vulnerable and piers are also critical for longer bridges. The study implies that without seismic design, integral precast multi-girder bridges are highly susceptible to pier shear failure, the probability of collapse is relatively high. The results also provide a solid basis for retrofit planning as well as for development of design concepts of newly built structures in moderate seismic zones.

Keywords Parametric seismic analysis · Seismic performance · Integral bridges · Multiple stripes analysis · Fragility analysis · Seismic reliability analysis · Moderate seismicity

1 Introduction

In high seismicity regions (such as the western coast of the United States (US), Japan, New-Zealand, the Mediterranean region of Europe, etc.), people are aware of significant earthquakes. Lessons learnt from previous devastating seismic events induced the

✉ József Simon
 simon.jozsef@epito.bme.hu

 László Gergely Vigh
 vigh.l.gergely@epito.bme.hu

[1] Department of Structural Engineering, Budapest University of Technology and Economics, Műegyetem rkp. 3-9. Kmf. 85., Budapest 1111, Hungary

🦎 Springer

improvement of seismic design and also the application and evaluation of retrofit strategies. In moderate or low seismic areas (eastern part of the US, northern and central parts of Europe, etc.), seismic risk mitigation efforts have lagged due to the fact that in these regions large earthquakes are infrequent and may not have been experienced for over a century while modern design methodologies and codes have been developed (Elnashai and Di Sarno 2008).

In the pre-Eurocode era, the majority of the bridges were not designed for seismic loads due to the lack of proper seismic provisions in many countries of moderate and low seismic zones. The introduction of Eurocodes EC8-1 and EC8-2 (CEN 2008a, b) created a new situation in these countries, which can be illustrated well through the situation of Hungary. As per the formal Hungarian standard ÚT (2004), only bridges with spans over 50 m had to be designed for seismic actions, regardless of their other—often more relevant—parameters. Moreover, the standard did not suggest any particular seismic design methodology, it only stated that the design shall be carried out "on the basis of acknowledged earthquake engineering principles". Along with the replacement of the national seismic regulations with the European standard, the seismic hazard of several European countries (e.g. Austria, Belgium, Czech Republic, Germany, Slovakia, Slovenia, Switzerland, etc.) was revised (Solomos et al. 2008). Prior to the revision, Hungary had been considered as a region of low seismicity throughout the past century. In 2006, a new peak ground acceleration (PGA) map (Fig. 1a) was released (Tóth et al. 2006) showing the moderate seismicity of the region with PGA values—for the hazard associated with 10 % probability of exceedance in 50 years—in the range of 0.08–0.15 g (similar to the Eastern US or North Italy, for instance).

The increase of seismic code requirement and the lack of seismic design raise the question whether highway bridges are able to retain their structural integrity or may suffer significant damage after a considerable seismic event. Experiences on existing and newly erected structures in the last decade (Vigh et al. 2006; Simon et al. 2015), and a parametric study on typical continuous girder bridges (Zsarnóczay et al. 2014) confirmed that a large portion of highway bridges may be vulnerable to earthquake loads in moderate seismic zones.

Figure 1b illustrates primary road (e.g. highways and autoroutes) bridges in Hungary. The number of precast multi-girder (PMG) bridges is nearly half of the 3200 bridges, besides, their estimated gross value is more than one third of the total value of the bridge stock. These numbers show their importance in the whole inventory, thus their failure due to the poor seismic performance may cause significant economic consequences. The popularity of PMG bridges appeared with the construction of highways in the 60's; and from the 70's, bridges are constructed as integrated continuous systems. The connections between the deck and the substructure (both at the abutments and piers) are monolithic,
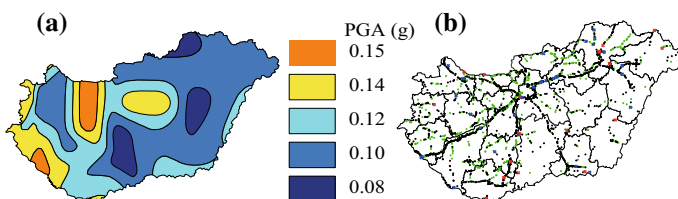

Fig. 1 a Seismic zone map of Hungary (10 % probability of exceedance in 50 years for PGA). **b** Primary road bridges in Hungary. Precast multi-girder bridges are marked with *black dots*

leading to different seismic behavior compared to bridges with simply supported beams and conventional bearings.

The popularity of such integral bridges is increasing, since the elimination of expansion joints and bearings lead to lower construction and maintenance costs. The largest number of integral bridges can be found in the US, where this typology has been used since the 1930s (Wasserman 2007). According to Kaufmann (2011), integral bridges are commonly used on the highways of Switzerland. An overview by White et al. (2010) comparing the European and US practice about integral bridges confirms that several other European countries (e.g. Austria, England, Finland, France, Ireland, Luxembourg, Germany, Sweden, etc.) employ this system as well; and it is also concluded that the deck is most commonly constructed with precast beams. Other realizations can be found e.g. in Japan (Nakamura et al. 2002; Akiyama and Kajikawa 2008) and in Australia (Connal 2004).

Comprehensive seismic performance evaluation of typical PMG highway bridges has been carried out e.g. in the US (Nielson 2005), Italy (Borzi et al. 2015), Greece (Moschonas et al. 2009), Turkey (Avşar et al. 2011) and Algeria (Kibboua et al. 2014), but to the best of the authors' knowledge, there is no such study on highway bridges in a moderate seismic zone of Europe. The results of the mentioned studies can be used to presume the seismic behavior of PMG bridges in moderate seismic zones; however, there are several reasons why they cannot be adapted directly: (1) in most low or moderate seismic zones, seismic design of bridges did not exist or underestimated the seismic effects; (2) the higher seismicity of the mentioned countries in Europe results in different design concepts and thus structural characteristics as well as details; (3) Hungarian PMGs are dominantly integrated continuous bridges, while simply supported versions are equally preferred in the mentioned regions; (4) differences in the relevant input parameters (e.g. pier height) affect significantly the seismic response; (5) the vulnerability of the examined bridge is highly dependent on the applied seismic actions (e.g. ground motions or response spectrum) which should be selected or determined in accordance with the seismic characteristics and site properties, thus results are expected to differ in moderate seismic zones.

State of the art seismic vulnerability evaluation techniques are based on analytical fragility curves created with either Incremental Dynamic Analysis (IDA) (Vamvatsikos and Cornell 2002) or Multiple Stripes Analysis (MSA) (Jalayer and Cornell 2009) using non-linear time-history analysis (NLTHA). Fragility curves are conditional probability statements giving the probability of reaching a particular limit state (LS) for an earthquake of a given intensity measure (IM) level. The fragility function can also be used with a seismic hazard curve to compute the probability of failure over a given reference period. Thus, fragility analysis is a useful tool for decision making, since the probability of a LS exceedance in a predefined time-window can be determined, retrofit decisions can be made regarding economical and financial aspects. Besides, fragility curves can be used for evaluation of other pre- and post-earthquake situations. With the comparison of the seismic performance via fragility curves, vulnerable bridge types and configurations can be highlighted, retrofit prioritization can be made. Fragility curves can also be used to assign a level of functionality of each bridge after a seismic event, which is essential for the determination of emergency routes and recovery planning (Basoz and Kiremidjian 1996).

The aim of this study is to evaluate the seismic performance of a wide range of different PMG bridge layouts. In a preliminary study (Simon and Vigh 2015), it was concluded that single span bridges are far less vulnerable, thus they are excluded from the evaluation. MSA is conducted to derive component and system fragility curves for multi-span configurations. Finally, the probability of failure for a 50 year reference period is calculated considering the highest and the lowest seismic areas of Hungary, well reflecting typical

European moderate seismic regions. Most of the earlier mentioned European countries can be characterized by moderate seismicity, thus the study provides useful results for these regions as well.

2 Description of PMG bridges

Figure 2a shows the general layout of PMG bridges. The construction steps are as follows. First, the substructure (piles, pile cap, abutments and piers, and finally the pier cap beam) is created, and vertical reinforcements are extended from the abutments and pier caps. After placing the precast beams, the last step is the installation of the reinforcements and construction of the monolithic joints and the concrete deck with cast-in situ concrete. PMG bridges with a few exceptions are built as continuous multi-span integrated systems. Semi-rigid flexural behavior characterizes the monolithic joints because of the closely spaced single or double vertical rebars (Fig. 2b, c). However, the flexural stiffness is negligible compared to those of the adjacent structural elements, it is best approximated as hinged (Fennema et al. 2005); thus the joints transfer horizontal forces only. Typical shear reinforcements are $\phi16/150$ at the abutment and $2\phi16/150$ at the piers. It should be emphasized that the shear reinforcement is fully embedded in concrete providing a passivating medium. However, if cracks develop, indirect water penetration may cause corrosion which should be taken into account by considering the remainder area of the reinforcement. Therefore, inspection of these joints are of high importance. Span length controls the distance between the I-shaped precast beam axes as well as the beam height. With statistical analysis of existing bridges, the structural height of the superstructure is determined as a function of the span length considering an equivalent slab and taking into account stiffness and mass properties (Fig. 2d). Piers are constructed as multi-column bents with column transverse spacing of 3–4 m. Longitudinal reinforcement ratio is usually ~ 1 %, while minimal shear reinforcement (mostly $\phi12/150$) is applied due to the low shear forces in conventional design situations (e.g. for traffic loads). The foundation system is mostly pile foundation, the assumed layouts of which for different deck widths are shown in
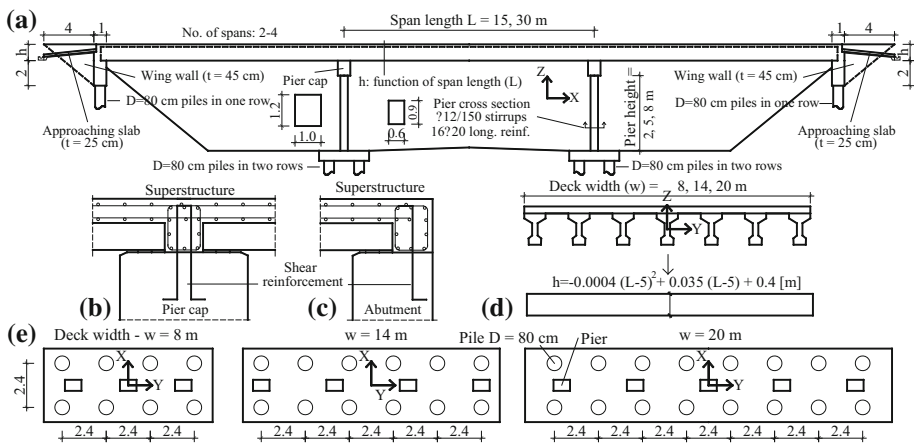

Fig. 2 General layout of PMG bridges: **a** side-view of the bridge; **b** monolithic joint at the pier; and **c** at the abutment; **d** typical cross-section; **e** applied pile foundation arrangements for different bridge widths

Fig. 2e. Although skew angle may significantly influence the seismic behavior, 82 % of bridges have skew angle under 20° (limit defined per EC8-2 to distinguish skewed and non-skewed bridges), thus the skewness is not taken into account in this study.

PMG bridges are popular on highways; cross section of the piers (0.6 m × 0.9 m) and the pier cap beam (1.0 m × 1.2 m) and the dimensions of the abutments (1.0 m × 2.0 m) are more or less the same for all structures for the efficient reusability of formwork. Accordingly, pier and pier cap cross-section, abutment geometry are considered fixed during the studies (see Fig. 2a). The input for the parametric study is determined with statistical analysis (Simon and Vigh 2015) of an existing road bridge database (HTA 2015). In Fig. 3a–d, histograms for the number of spans, deck width, span length and pier height are illustrated for multi-span bridges, respectively. The figure confirms that it is sufficient to examine 2-, 3- and 4-span configurations only, covering more than 90 % of the bridges. In the parametric study, deck width is fixed to three values of 8, 14 and 20 m. Actual span length ranges between 5 and 35 m; however, since shorter bridges are less likely to be vulnerable, two reasonable span lengths are applied for the parametric study: 15 and 30 m. The input parameters are summarized in Table 1. The notations for different configurations are also indicated in the table, e.g. a 14 m wide (W) 3-span (S) bridge with 5 m pier height (P) and 30 m span length (L) is referred to as W14S3P05L30.

The referred bridge database incorporates yearly updated data on the condition of the bridges, confirming that structural elements of the PMG bridges are in good or excellent condition; besides, no significant cracks in the monolithic joints were reported. This is an expected condition, since these structures are on primary roads, where maintenance and planned recovery are of high priority and considered as a basic requirement. Accordingly, strength or stiffness deterioration of the structural members are not accounted for in the numerical model presented herein.

3 Numerical modeling

3.1 General description

Three dimensional beam-element model (Fig. 4) is created in OpenSees (McKenna et al. 2010). The superstructure, piers, abutments and pier caps are modeled with two-node 3D beam elements with 6 degrees of freedom per node. The beam elements are placed in the center of mass, the eccentricity between the member axes is modeled with rigid elements. A typical mesh size of 0.25 m is found sufficient to achieve results with an acceptable accuracy for all the examined configurations. The mass of the structure and the additional dead load (450 kg/m^2 pavement and 700 kg/m railing) are lumped into nodes.
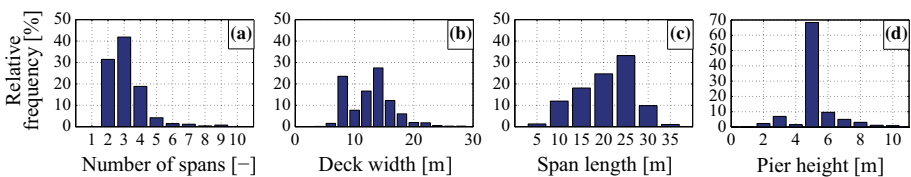
Fig. 3 Histograms in % for multi-span bridges: **a** number of spans; **b** deck width; **c** span length; **d** pier height

Table 1 Input parameters for the parametric study and notations for different configurations

	Width [m]	Number of spans [-]	Pier height [m]	Span length [m]
Values	8, 14, 20	2, 3, 4	2, 5, 8	15, 30
Notations	W08, W14, W20	S2, S3, S4	P02, P05, P08	L15, L30
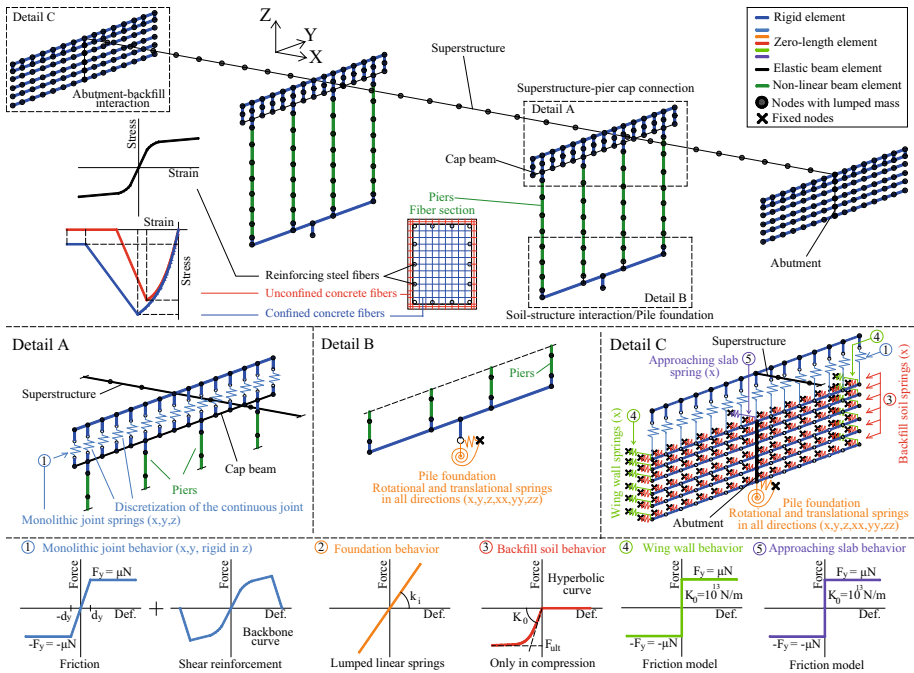
Fig. 4 Three dimensional beam element model in OpenSees

3.2 Superstructure and pier cap beam

The superstructure and the cap beam is expected to remain elastic during an earthquake as it is concluded in the preliminary analysis (Simon and Vigh 2015), therefore linear elastic behavior is assigned to these components (*elasticBeamColumn* element).

3.3 Superstructure–substructure joints

The superstructure-substructure joints have a significant effect on the seismic behavior, since their characteristics define the amount of internal forces transferred from the superstructure to the abutments and piers. Moreover, failure of these components may lead to unseating of the girders causing severe damage in the bridge system. To account for the cyclic non-linear behavior of the joints, non-linear spring elements (*ZeroLength* element) with appropriate constitutive models are assigned in specific degrees of freedom. The continuous monolithic joints are approximated with discrete contact points along the

transverse direction with concentrated constitutive models calculated from the corresponding contact lengths (Fig. 4 detail A and C). The joint is assumed to work as a hinge, therefore it is sufficient to characterize only the lateral behavior (i.e. the relationship between the shear forces and lateral deformations). During the rotation of the joint, cracks may appear on the concrete–concrete surface. Reliable estimation of the concrete shear strength thus cannot be given. Accordingly, it is assumed that the horizontal forces are transferred only by the shear reinforcements and the friction between the two concrete surfaces. The latter is modeled with a bi-linear model (*Steel01* material), where the yield force (F_y) is calculated as the product of the normal force acting on the joint surface and the frictional coefficient; and d_y is determined in accordance with FIB (2008) using the normal stress on the contact surface:

$$d_y[\text{mm}] = 0.15\sqrt{\sigma_N[\text{MPa}]}, \tag{1}$$

The rebar behavior is modeled by *Pinching4* material. Based on laboratory test results of pinned connections with 2ϕ16 vertical rebars (Psycharis and Mouzakis 2012), material model calibration is carried out to model the cyclic behavior of the shear reinforcement. The input parameters of the material model are the force–deformation points of the monotonic backbone curve (available from the tests); parameters controlling the pinching behavior (*rD, rF, uF*); the degradation of the unloading stiffness (*gK1-gK4, gKlim*), the reloading stiffness (*gD1-gD4, gDlim*) and the strength (*gF1-gF4, gFlim*); and the last two parameters (*gE, dmgType*) define the maximum energy dissipation under cyclic loading and the type of algorithm for damage estimation. Energy-based damage indices are defined as a function of both displacement history and energy accumulation. Due to the relative large number of 19 unknown parameters and the high non-linearity of the problem, a heuristic optimum search method, the genetic algorithm (Goldberg 1989) is used. The applied fitness function is calculated from the weighted sum of square errors of the tested and calculated load values. The test results and the results of the calibrated material model subjected to the same load protocol are compared in Fig. 5a, confirming that the calibrated model reliably captures the nonlinear cyclic behavior of the detail. The calibrated model parameters are shown in Fig. 5b.

3.4 Piers

Piers are modeled with nonlinear beam elements (*dispBeamColumn* element), material nonlinearity is taken into account with fiber sections, while geometric nonlinearity is also

(b)

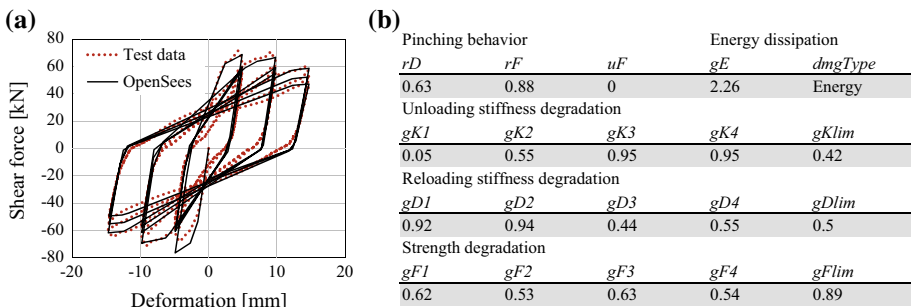| Pinching behavior			Energy dissipation	
rD	rF	uF	gE	dmgType
0.63	0.88	0	2.26	Energy
Unloading stiffness degradation				
gK1	gK2	gK3	gK4	gKlim
0.05	0.55	0.95	0.95	0.42
Reloading stiffness degradation				
gD1	gD2	gD3	gD4	gDlim
0.92	0.94	0.44	0.55	0.5
Strength degradation				
gF1	gF2	gF3	gF4	gFlim
0.62	0.53	0.63	0.54	0.89

Fig. 5 a Comparison of the test results and the calibrated Pinching4 material model. **b** Calibrated parameters

incorporated. Uniaxial constitutive models assigned to the fibers are the Scott-Kent-Park concrete model (*Concrete01* material) and the Giuffré–Menegotto–Pinto reinforcing steel model (*Steel02* material) (see Fig. 4). Confined concrete properties are calculated per EC8-2 Annex E. It should be emphasized that due to the low shear reinforcement ratio ($\sim$0.2 %), the increase of strength and ductility of the confined concrete is not significant (<5 %).

3.5 Abutment and backfill soil system

The abutment can be regarded as a rigid block, stability failure is more possible than failure due to inadequate strength. Therefore, abutments are modeled with simple linear elastic behavior (*elasticBeamColumn* element, Fig. 4 detail C). The backfill soil under compression provides extra support in addition to the stiffness of the abutment. Its influence on the seismic response can be dominant in the longitudinal direction (Sextos and Taskari 2008; Kappos and Sextos 2009). As part of the Caltrans seismic research program, full-scale abutment field experiments were conducted (Maroney 1995). The test results showed hyperbolic force–deformation behavior of the abutment-backfill soil system subjected to monotonic longitudinal loading (Shamsabadi et al. 2007). This hyperbolic behavior is implemented in the model through compression-only non-linear spring elements (*ZeroLength* element) with adjusted spring characteristics (*HyperbolicGap* material). One end of the springs is attached to the nodes of a rigid grid modeling the surface of the abutment; the other end is attached to fixed nodes (Fig. 4 detail C). The initial stiffness of the hyperbolic curve is calculated per Caltrans (2013) from an initial stiffness value (K_i) determined for the entire width (w) of the bridge. The stiffness is adjusted to a typical backwall height ($H = 2$ m) and lumped to the abutment surface nodes proportionally to the corresponding areas (A):

$$K_0 = K_i w (H/1.7\,\mathrm{m})/A. \tag{2}$$

The ultimate force is lumped into the surface nodes in the same way, where 368 kPa maximum passive soil pressure is used for dynamic loads per Caltrans (2013):

$$F_{ult} = 368\,\mathrm{kPa}\,(H/1.7\,\mathrm{m}) \cdot A. \tag{3}$$

The progressive compaction (ratcheting) of the backfill soil is a typical behavior of integral abutment bridges, especially in case of highway overpass bridges comprised between two embankments (Franchin and Pinto 2014). The cyclic deformations caused by either thermal movements or—more importantly—seismic effects lead to increasing stresses in the abutments and the monolithic joints. The above presented plastic *HyperbolicGap* material model is capable of capturing the accumulating soil deformations and therefore the mentioned ratcheting effect.

The participating mass of the backfill soil is also incorporated. The mass is calculated considering the critical length (L_c) of the embankment according to Zhang and Makris (2002):

$$L_c \cong 0.7\sqrt{SB_cH} \tag{4}$$

where B_c and B_b are the crest and base width (at the bottom of the backwall) of the embankment, and $S = 2H/(B_b - B_c)$ is its slope. The participating mass is lumped to the abutment surface nodes.

In case of the approaching slab and the wing walls, both the inertial mass and the developing frictional forces at the backfill soil contact surfaces are taken into consideration (see Fig. 4 detail C). The approaching slab is assumed to be 4 m long and 0.25 m thick, thus its mass is calculated as 20 t, 35 t and 50 t for 8, 14 and 20 m deck widths, respectively; while the geometry of the wing wall is independent of the width, it is 2 m × 4 m × 0.5 m with a mass of ∼ 10 t, each. The frictional resistance is modeled with bilinear springs (*zeroLength* element) with rigid initial stiffness (10^{13} N/m), where the yield force is calculated using a frictional coefficient of 0.4 (Mitoulis 2012). The normal force on the contact surface is determined from the weight of the approaching slab and an assumed underlying soil of 1 m with 18 kN/m^3 unit weight; while at the wing wall, it is calculated from the lateral earth pressure of the backfill soil. The resulting yield force at the approaching slab is 375, 655 and 936 kN for the widths of 8, 14 and 20 m, respectively; while the yield force at the wing wall is 57.5 kN. The mass and the springs of the approaching slab are assigned to the node of the abutment at the height of the slab (0.5 m below the top of the deck), while those of the wing walls are distributed along the vertical edges (positions of the wing walls) of the rigid grid of the abutment, as shown in Fig. 4 detail C.

3.6 Foundation

The seismic response of a flexibly-supported structure fundamentally differ in several ways from those calculated assuming foundation on a rigid ground. Former practice usually neglected the effects of flexible support, while fragility analysis of bridges are also often conducted with rigid boundary conditions (Borzi et al. 2015; Avşar et al. 2011). The dynamic impedance of the soil-foundation system can be approximated through assemblies of springs, dashpots and fictitious masses (Wolf 1985). The complex impedance is frequency-dependent, where the complex part represents radiation damping in the soil. As a conservative approach, both radiation and material damping of the soil is neglected in this study. Linear springs are used (*ZeroLength* element) to take into consideration the translational and flexural stiffness of the pile foundation (Fig. 4 detail B). The vertical stiffness of an individual pile is determined as the initial stiffness of a simplified tri-linear behavior, representing the combined behavior of skin friction and tip resistance; the horizontal stiffness is estimated according to EC8-5 Annex C (CEN 2009). The translational and rotational stiffness of the foundations are calculated directly from the vertical and horizontal stiffness of the individual piles considering the actual layout of the pile foundation system. Since PMG bridges are built with monolithic joints, the seismic resistance is provided by both piers and abutments. In this case, the use of lower and upper bound estimates of the soil stiffness is recommended to obtain conservative demands for both the internal forces and deformations. Table 2 illustrates representative stiffness values considering the Young modulus of the soil as either 10 MPa (lower) or 100 MPa (upper) (typical range from soft to stiff clay and from loose to compact sand).

3.7 Loading

Non-linear analysis is carried out in two steps. First, to model the initial (pre-earthquake) state of the bridge, the gravity loads are applied, and a linearly increasing loading is used at the abutments considering at-rest earth pressure to model that the backfill is in compression. The accumulated deformations caused by the thermal effects during the bridge service is not considered for simplification. The presented comprehensive study aims at

finding global tendencies related to solely the seismic action, regarding the most vulnerable configurations and bridge components as well as the reliability of the structures. It should be emphasized, however, that in some cases progressive build-up of earth pressures behind the abutments may reach considerably large levels at the occurrence of seismic actions (England et al. 2000). This effect shall be investigated when a specific configuration is evaluated in detail.

After reaching equilibrium, the second step is to apply the tri-component seismic input (see Sect. 4.3) for non-linear time-history analysis. The time history analyses are conducted using an initial time step of 0.0025 s and it is further reduced when needed due to numerical convergence issues. 5 % Rayleigh damping is used, the damping coefficients are calculated considering the first two vibration modes. Since these structures are relatively stiff, yielding of the system leads to considerable increase in the vibration periods. Therefore, calculating the damping matrix with the initial stiffness of the system results in overestimated damping (Charney 2008). For this reason, the damping matrix is constructed with the current stiffness matrix in each iteration step.

3.8 Sensitivity analysis—effect of various modeling assumptions

Prior to the fragility analysis, influence of 9 modeling assumptions is investigated by comparing representative demands to the reference model M1 (presented above). Model M2 employs rigid connections. Model M3 uses a simplified bi-linear backfill force–deformation relationship (proposed by Caltrans) instead of the originally used hyperbolic one. M4 neglects the mass of the backfill soil. M5 and M6 neglect the strength and mass of the approaching slabs; and M7 neglects both. M8 and M9 do not account for the strength and the mass of the wing walls; and M10 does not include the wing walls at all.

Figure 6 illustrates representative demands of the W14S3P05L30 configuration subjected to a high intensity (PGA = 6.5 m/s^2) shaking in the longitudinal direction. The importance of modeling the non-linear joint behavior is apparent: the results indicate that high seismic demands may cause strength degradation of the shear reinforcement at the abutment joint. Eventually, the shear resistance may be drastically reduced, only frictional forces develop. This degradation can lead to the redistribution of the internal forces: pier

Table 2 Stiffness values of the foundation springs

Span length	Stiffness estimation	Abutment						Pier					
		k_x 10^9 N/m	k_y	k_z	k_{xx} 10^9 Nm/rad	k_{yy}	k_{zz}	k_x 10^9 N/m	k_y	k_z	k_{xx} 10^9 Nm/rad	k_{yy}	k_{zz}
L15	Lower	0.28	0.28	0.56	11.44	1.99	10^4	0.56	0.56	1.13	22.88	5.61	10^4
	Upper	1.72	1.72	0.56	12.99	3.54		3.43	3.43	1.13	25.99	8.71	
L30	Lower	0.28	0.28	0.94	17.74	1.99		0.56	0.56	1.88	35.48	6.68	
	Upper	1.72	1.72	0.94	19.29	3.54		3.43	3.43	1.88	38.59	9.79	

k_x, k_y and k_z denote translational stiffness along the x, y and z axis (see Fig. 4); while k_{xx}, k_{yy}, k_{zz} represent rotational stiffness values about the same axes, respectively

demands and shear forces at the pier joint may be significantly increased compared to the rigid connection model.

Figure 7 presents the effect of modeling assumptions on the most important seismic demands. In this case, NLTHAs are carried out in the longitudinal direction with 14 artificial records (matched to the EC8 Type 2 standard spectrum considering soil type C), then the average of the demands are compared to those of the reference model M1. A shorter (30 m) and a longer (120 m) configuration are investigated for different pier heights (2 and 8 m) and intensity levels (PGA of 0.25 and 0.50 g). The figure confirms the great influence of the joint behavior. Using a rigid connection underestimates all the examined demands at the lower intensity level (0.25 g). However, when the abutment joint yields, certain demands may be decreased (e.g. pier shear due to the increased fundamental period; backfill soil deformation due to the decreased transferred lateral forces) and therefore overestimated with the rigid connection model M2. Modeling the backfill soil with bi-linear behavior (model M3) yields conservative estimation, except for the abutment joint deformations. By neglecting the participating mass of the backfill soil (model M4), all the relevant demand parameters of shorter configurations are underestimated by 10–25 %; while its effect is negligible for longer bridges. Neglecting the strength (models M5 and M8) and the mass (models M6 and M7) of the approaching slab and the wing walls result in overestimated (5–10 %) and underestimated (5–10 %) demands, respectively; however the total effect (models M7 and M10) is less significant and can even be neglected for longer bridges. In conclusion, the joint model and the participating mass of the backfill soil have significant influence on the seismic behavior, however latter is negligible for longer bridges.

4 Reliability model and fragility analysis procedure

4.1 Applied analysis method

The study adopts MSA for fragility analysis for two major reasons: (1) it is proved to be more efficient than IDA for a given number of structural analyses (Baker 2015); (2) it allows for the use of different ground motion sets at varying intensity levels, to represent the altering characteristics of low and high intensity shaking. Steps of the MSA are presented in Fig. 8. At each intensity level a number of ground motions are selected for each horizontal direction. Maximum demands are registered during NLTHA. Assuming
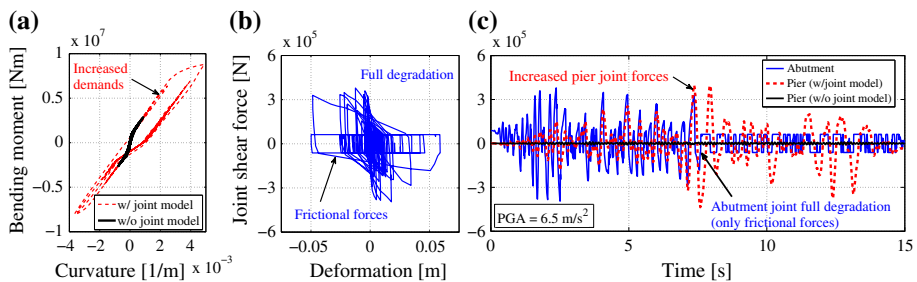

Fig. 6 NLTHA results with or without modeling the joint behavior for the W14S3P05L30 configuration. **a** Pier moment–curvature diagram. **b** Abutment joint behavior. **c** Abutment and pier joint shear forces
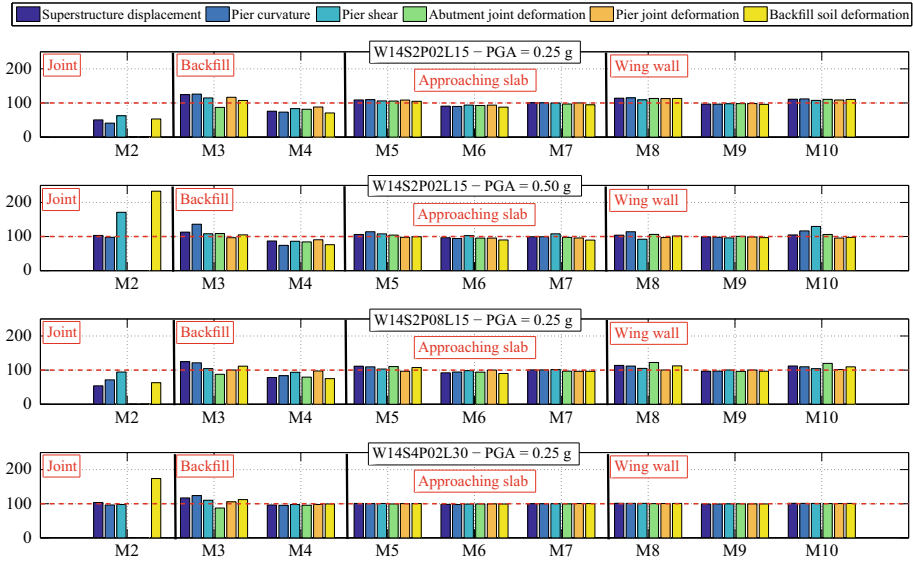
Fig. 7 The effect of different modeling assumptions (M2–M10) compared to the M1 reference model in %

lognormal (LN) distribution, median and coefficient of variation (CoV) of the relevant demand parameters (*D*) are calculated at each IM level. A single fragility point at an intensity level is obtained as follows:

$$P[(D > C_{LSi})|IM] = \int_0^\infty P(D > \alpha|IM)P(C_{LSi} = \alpha)d\alpha, \tag{5}$$

where *D* is the calculated seismic demand; C_{LSi} is the capacity associated with the *i*th LS; the second function is the probability density function of the capacity; and α denotes the
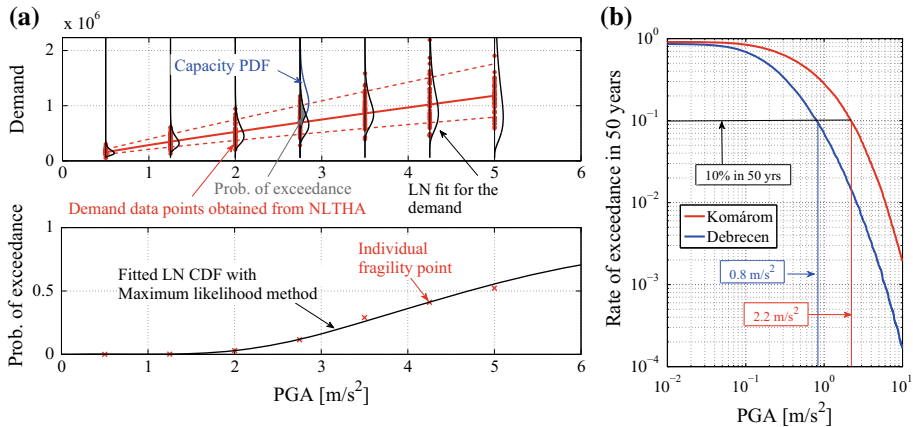

Fig. 8 a Multiple stripes analysis procedure. **b** PGA hazard curve for the area of Komárom and Debrecen considering soil type C and a 50 year reference period

integration over the demand parameter. As the last step, maximum likelihood method is invoked to obtain fitted LN cumulative distribution function (CDF) estimation of the fragility curve (Baker 2015). Afterwards, the seismic risk associated with LS_i can be computed as:

$$p_i = \int_{IM} P[(D > C_{LSi})|IM]d\lambda(IM), \tag{6}$$

where $d\lambda$ is the derivative of the hazard curve. Reliability index β is computed for the evaluation and comparison of the performance of different configurations:

$$\beta_i = -\phi^{-1}(p_i). \tag{7}$$

The component fragility curves are useful to highlight critical components, and to calculate the probability of component failure. However, reliability model of the bridge structure as a whole shall be considered as system of (failure) components. It is assumed that bridges compose series systems (system failure is associated with the failure of any component). Using first-order reliability theory, a simple lower and upper bound on the system fragility (P_{sys}) can be determined for an m-component system with P_i component probabilities at a given IM level:

$$\max_{i=1:m} P_i \le P_{sys} \le 1 - \prod_{i=1}^{m}[1 - P_i]. \tag{8}$$

The lower bound represents a system where the components are fully stochastically dependent (un-conservative estimate), while the upper bound assumes that the components are all statistically independent (conservative estimate) (Nowak and Collins 2000). Additionally, Monte-Carlo (MC) simulation is applied to give a better estimation for the system fragility curve. The joint distribution of the demands and capacities are assumed to be multivariate LN (MLN) distributions (Nielson 2005). At each IM level, the marginal distribution of the component demands are obtained with MSA, then the cross-correlation is computed to fully describe the distribution of the demands. Since the correlation between the component capacities is not known, two cases are examined: full or no correlation of the capacities. The idea of the simulation is to generate a large number of random samples from the demand and capacity MLN distributions, allowing that the P_{sys} is determined by taking the ratio of the cases of failure and the number of simulated cases. The calculation is repeated at various IM levels to obtain the individual points of the system fragility curve.

Besides MSA and IDA, Cloud Analysis is often used in literature (e.g. Nielson 2005; Padgett 2007; Avsar et al. 2011) to create analytical fragility curves, where unscaled recorded ground motions are applied for NLTHA having the benefit of maintaining the original characteristics (frequency and energy content) of the recorded earthquake. If the maximal structural responses are plotted against a selected IM, a cloud of points is obtained (record selection is usually arbitrary; see Fig. 9c, d). Note that MSA can be regarded as a special Cloud Analysis, where the maximal structural responses form into line (see Fig. 9a, b) at the chosen conditioning IM levels (PGA in this study). With regression analysis, a Probabilistic Seismic Demand Model (PSDM) can be obtained providing the median (S_D) and the lognormal standard deviation (LNSTD) (β_D) of the demands as the function of the IM. Typically, a power law is used to describe the PSDM:
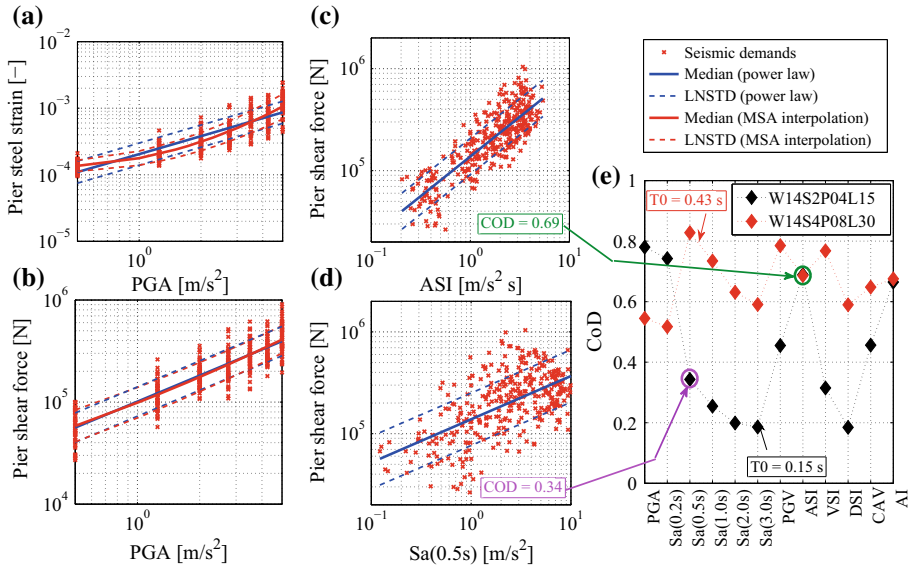
Fig. 9 **a–d** Structural responses against various IMs for the W14S2P02L15 configuration. **e** Coefficient of determination values showing the appropriateness of different IMs

$$S_D = a\,IM^b \tag{9}$$

The fragility function can be obtained with the median (S_C) and LNSTD of the capacity (β_C):

$$P[(D > C_{LS})|IM] = \phi\left(\ln(S_D/S_C)/\sqrt{\beta_C^2 + \beta_D^2}\right). \tag{10}$$

The presented power law leads to a linear approximation of median values in the log–log space and assumes a constant LNSTD. Figure 9a, b illustrates some calculated demands of the W14S2P02L15 configuration. In some cases (e.g. pier shear forces) the linear approximation resulted from the application of the power law is correct; however, it is not appropriate to describe elements with high plastic deformations at higher intensity levels (e.g. the reinforcing steel strains). Moreover, the slope of the linear curve in the log–log space is highly dependent on the intensity levels considered. On one hand, if only records with lower intensities are applied during the analysis, the linear approximation underestimates the demands at higher IM levels. On the other hand, too high dispersion is assumed at low intensities due to the constant LNSTD along the entire IM range if the plastic deformations are dominant. The improper characterization of the seismic demands may lead to either conservative or non-conservative estimation of the fragility curve. The advantage of MSA is that the median and LNSTD values can be calculated at each IM level providing a better estimation for the PSDM, and thus for the fragility curves as well.

4.2 Selection of the main intensity measure

As noted by Bradley (2012a), the seismic demand hazard, therefore the calculated probability of failure is independent of the chosen IM if hazard consistent ground motions are

selected (see in Sect. 4.3). However, it is still recommended to use an IM that correlates well with the calculated seismic demands in order to minimize the uncertainty associated with the simplified approach of using only one scalar parameter to describe the seismic action. Besides, the presented results are also useful to provide guidance for the case of arbitrary record selection (e.g. for Cloud Analysis), where the reliability of the derived fragility curves are strongly dependent on the considered IM. The evaluation of various IMs—such as PGA, spectral acceleration (Sa) at 0.2, 0.5, 1.0, 2.0 and 3.0 s, peak ground velocity (PGV), acceleration spectrum intensity (ASI), velocity spectrum intensity (VSI), displacement spectrum intensity (DSI), cumulative absolute velocity (CAV) and Arias intensity (AI)—is carried out as follows. The PSDM from Eq. (9) is applied and the coefficient of determination (CoD) of the regression is used for comparison. Higher CoD values represent more appropriate IMs. For instance, ASI with a CoD value of 0.69 is a better estimator of the seismic demands than Sa(0.5 s) (CoD = 0.34) for the W14S2P02L15 configuration (Fig. 9c, d). CoD values of other IMs for pier shear forces (other demands have the same tendency) are presented in Fig. 9e for the stiffest and most flexible examined bridges. As confirmed by Fig. 9e, the optimal IM is highly correlated with the first fundamental period (T_0) of the structure. PGA, ASI and AI represent well the demands of the stiff bridge ($T_0 = 0.17$ s); while with the increase of the fundamental period ($T_0 = 0.42$ s), Sa values close to T_0 as well as PGV and VSI become more dominant. Note also that ASI and AI perform well for both configurations.

On the basis of the results, PGA is selected as the IM in this study for three main reasons: (1) the applied record selection method in this study ensures that the demand hazard will be statistically independent of the conditioning IM (note that the conditional probability, therefore the fragility curves may differ); (2) it is concluded that PGA represents well the demands of relatively stiff PMG bridges (which is in accordance with the results of Nielson (2005)) and could be considered as satisfying the criterion of correlating well with more flexible bridges as well; (3) the comparison between fragility curves are easier with a general IM such as PGA; besides, PGA is the most widely used IM, thus interpretation of the results is convenient. 7 (PGA = 0.5:0.75:5 m/s^2) intensity levels are chosen and 50 tri-directional ground motions (two horizontal and one vertical component) are selected for each level in all cases considering soil type C (average shear wave velocity $v_{s30} < 360$ m/s).

4.3 Ground motion selection

A state of the art General Conditional Intensity Measure (GCIM) approach (Bradley 2010, 2012b) is adopted for ground motion selection. The idea of GCIM is similar to that presented in (Baker 2011), deriving the distribution of a vector of IMs conditional on the main IM from their joint distribution. The novelty of the GCIM method is that the IM vector can consist of not only spectral intensities but also other IMs such as energy content or duration measures. Since the marginal distribution of the IMs are assumed to be LN, it is also assumed that the joint distribution is LN as well. Thus, correlation structure between each IM and the ground-motion prediction models (GMPM) for the marginal distributions shall only be computed. Due to the fact that only a finite number of 50 recorded ground motions are needed, proper selection of the theoretical distribution can be judged on the basis of goodness-of-fit tests, such as Kolmogorov–Smirnov (KS) test as proposed by Bradley (2012b). Firstly, a number of random realizations are generated from the theoretical distributions, then the selection is done by choosing ground motions for each realization with the smallest residual. Since the distributions of the realizations are

consistent with the original GCIM distribution (they have the same mean, standard deviation and correlation structure), it is likely that properly chosen ground motions are consistent as well and they pass the KS test.

The record selection is carried out for the area of Komárom and Debrecen, selecting three component ground motions, considering soil type C and using the strong motion database of the Pacific Earthquake Engineering Research Center (PEER 2015). The selection is based on the geometric mean of the IMs of both horizontal directions, while the third vertical component is that of the selected record. As it is mentioned above, PGA is chosen as conditioning IM, and also Sa at $T_0 = \{0.1:0.1:0.8,1.0,2.0\}$ s are considered to account for ground motion intensity over a wide range of vibration periods; and additionally, ASI, PGV and VSI are included in the IM vector regarding that the examined bridge configurations are either acceleration or velocity dependent structures. These parameters represent peak responses, however, to describe cumulative phenomena (which may be important for the plastic deformations of the backfill, joints and piers at higher intensities), cumulative absolute velocity (CAV) and significant durations (D_{s575} and D_{s595}) are also incorporated. Therefore the IM vector consists of 17 elements: {PGA, Sa(T_0), PGV, ASI, VSI, CAV, D_{s575}, D_{s595}}. According to Bradley (2012b), the importance of different IMs should be taken into account by assigning different weights to them. The weights are set equally, thus the total weight of the most important IMs related to peak responses is ~ 0.8, while a total weight of ~ 0.2 is assigned to the other IMs associated with cumulative behavior. The GMPM for PGA proposed by Akkar and Bommer (2010) is applied; references to other GMPMs and the equations to calculate the correlation structure are summarized elsewhere (Bradley 2012b).

The conditional distribution is assigned to specific hazard levels, thus at each intensity level a different set of ground motions can be selected reflecting the characteristics of expected earthquakes with the given intensities. An example conditional distribution for some selected IMs for the main IM level of 2.19 m/s^2 PGA (hazard level of 10 % in 50 years) along with the KS bounds and the empirical CDF of the selected records can be seen in Fig. 10a, while Fig. 10b illustrates the spectrum of the selected records.

4.4 Damage limit states

Three damage limit states as suggested by Priestley et al. (1996) are considered. The damage states can be associated to levels prescribed in EC8-3 (CEN 2011a): Damage Limitation (LS1), Significant Damage (LS2) and Near Collapse (LS3). As per EC0 (CEN 2011b), the capacities of the bridge components are assumed to follow LN distribution. The definitions of the limit states and the assigned median and CoV values for each component are summarized in Table 3.

4.5 Uncertainties applied during the analysis

MSA can be regarded as a simplified MC simulation, where the capacity distribution is known and the distributions of the demands are determined independently from a reasonably large number of time-history analyses at each intensity level. The uncertainty of the demands are controlled mainly by the seismic load. However, to take into account other uncertainties in the phase of determining the demands, material properties and other input parameters are considered as random variables (Table 4). For each time-history analysis, a random sample is used to create the numerical model of the bridge.
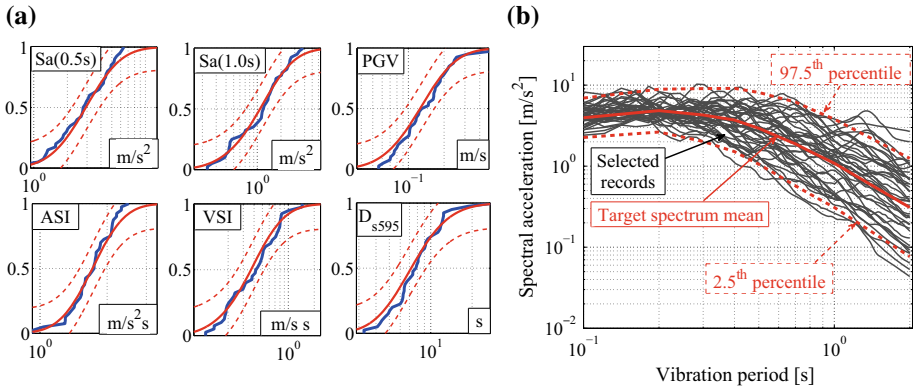
Fig. 10 Record selection for the Komárom area. **a** Theoretical distribution of some IMs conditioned on PGA (*solid red line*). *Red dashed line*: KS bounds (0.1 confidence level); *solid blue line*: empirical distribution of the selected records. **b** Acceleration response spectra of the selected records

5 Results

5.1 Modal analysis results

Typical first vibration modes and fundamental periods are illustrated in Fig. 11a for two extreme cases (regarding the main structural parameters; W08S2P02L15 and W20S4P08L30 configurations). The figure shows that the structure is relatively stiff in the transverse and the longitudinal directions, the first vibration mode is associated with the vertical movements of the superstructure. Similar tendencies can be observed in case of other configurations with fundamental periods T_0 within the range of 0.15–0.45 s. Figure 11b depicts the first dominant vibration periods in both lateral directions confirming the high stiffness in the transverse ($T_0 = 0.1$ to 0.35 s) and even higher stiffness in the longitudinal direction ($T_0 = 0.05$ to 0.10 s). Typical values of the T_B and T_C corner periods (which determine the constant plateau of the EC8 standard Type 2 response spectrum) are also indicated in Fig. 11b. Except for the transverse vibration periods of longer, more flexible bridges, typical vibration periods in most cases fall within the range specified by T_B and T_C periods, indicating that high base shear forces can be expected and that these bridges are possibly vulnerable to seismic actions.

5.2 Calculated demands

The tendencies and the order of magnitude of the seismic demands are illustrated through the MSA results of a typical highway overpass configuration with either a shorter (2 m) or a higher (8 m) pier (Fig. 12). The results highlight that the seismic demands are highly dependent on the relative stiffness of the abutments and piers. The demands at the piers (e.g. pier steel strain, concrete strain, shear forces and pier joint deformations) may be 3–10 times higher if the piers are shorter. The tendency is reversed at the abutments, the relevant demands (e.g. backfill soil deformations, abutment joint deformations) may be increased (2–7 times) in case of higher, more flexible piers.

In the range of typical design PGA values in moderate seismic areas (1–2.5 m/s²), pier yielding and the spalling of concrete are not expected, median steel strain and concrete

Table 3 Limit states and associated capacities

Component	Measure	Definition			Median			CoV[a]		
		LS1	LS2	LS3	LS1	LS2	LS3	LS1	LS2	LS3
Pier flexural	Steel or concrete strain	Yielding of rebars	Spalling of concrete	Crushing of concrete	0.28 %	0.3 %[b]	VA[c]	0.25	0.30	0.35
Pier shear[d]	Shear force	Shear failure	Shear failure	Shear failure	VA[e]	VA	VA	0.25	0.25	0.25
Monolithic joint longitudinal	Deformation	Yielding	Strength degradation	Unseating	2 mm	50 mm	300 mm	0.25	0.30	0.35
Monolithic joint transverse	Deformation	Yielding	Strength degradation	Unseating	2 mm	50 mm	450 mm	0.25	0.30	0.35
Backfill soil[f]	Deformation	Yielding	Minor damage	Abutment instability	30 mm	60 mm	300 mm	0.25	0.30	0.35

VA various values for different configurations

[a] In case of shear failure, the CoV value is assigned according to Biskinis et al. (2004). The other LSs are determined in a prescriptive manner (the thresholds are defined by the analyst) with assigned CoV values of 0.25, 0.30 and 0.35 (Nielson 2005)

[b] Priestley et al. (1996)

[c] Determined with moment–curvature analysis of the pier cross-section. Typically ∼ 0.45–0.50 %

[d] Brittle failure mode, only one limit state is defined

[e] Calculated per Priestley et al. (1996) considering the contributions from concrete resistance, axial force and transverse steel. E.g. the median shear resistance of a typical highway bridge configuration (W14S3P05L30) is 890 kN

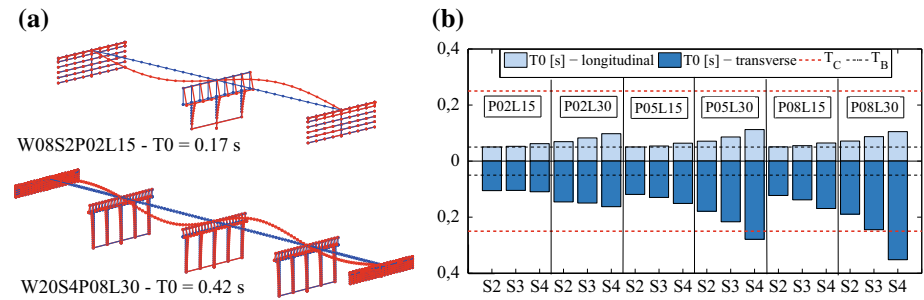[f] Capacity values are in accordance with EC8-2 (yielding, damage control limit, excessive deformation)

Fig. 11 **a** Typical first vibration modes. **b** Longitudinal and transverse vibration periods for W14 bridges

Table 4 Random variables applied to sample input for the numerical model

Variable	Distribution	Mean/median/min	STD/CoV/max	Reference
Pier cross section	Uniform[a]	VA	±20 mm	–
Pier height	Uniform	VA	±50 mm	–
Superstructure mass	Normal	VA	0.1	Nowak and Collins (2000)
Reinforcement ratio	Uniform	1 %	±0.3 %	–
Concrete compressive strength	Lognormal	28.8 MPa	0.15	JCSS (2001)
Reinforcing steel yielding	Normal	598 MPa	0.1	JCSS (2001)
Friction coefficient (concrete–concrete)	Uniform	0.4	±0.1	–
Foundation stiffness[b]	Uniform	VA	VA	Nielson (2005)
Backfill soil (Ki) stiffness[c]	Uniform	14.4 kN/mm/m	28.8 kN/mm/m	Caltrans (2013)
Backfill soil mass[d]	Uniform	VA	VA	–
Earthquake direction	Uniform	$\pi/4$ rad	±$\pi/4$ rad	Nielson (2005)

VA various values

[a] When sufficient information on probability distributions is not available, uniform distribution with reasonable upper and lower limits is assumed to roughly account for uncertainty (Nielson 2005)

[b] Uniformly distributed between the lower and upper values presented in Table 2

[c] Based on the upper and lower value of 14.4 and 28.8 kN/mm/m proposed by Caltrans (2013)

[d] The lower and upper bounds are calculated considering the slope (S) of the embankment as either 1/3 or 2/3. E.g. the lower and upper bound of the mass is 147 t and 225 t for 14 m deck width

strain are well under 0.28 and 0.3 %, respectively. Pier shear forces are only 100–400 kN in case of high piers, and are in the range of 400–1500 kN for shorter piers. For comparison, the median shear resistance of the two examined configurations are ~ 1100 and ~ 900 kN for 2 and 8 m pier height, respectively. This highlights the high vulnerability of bridges with short piers. The backfill soil deformations are only 1–4 mm, thus damage of this component is unlikely. It can also be observed that the deformations are not constantly increasing with the intensity, because yielding of the abutment joints decreases the horizontal forces transferred to the backfill soil. The abutment joint demands are considerably higher than those of the pier joints, especially in the longitudinal direction. Yielding is expected in both directions at the abutment, while yielding in the transverse direction at the
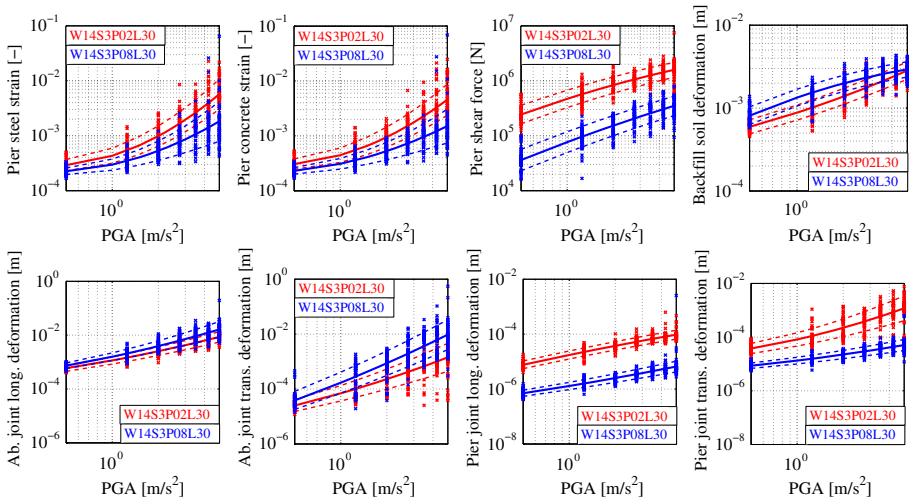
Fig. 12 Representative seismic demands of the W14S3P02L30 and W14S3P08L30 configurations
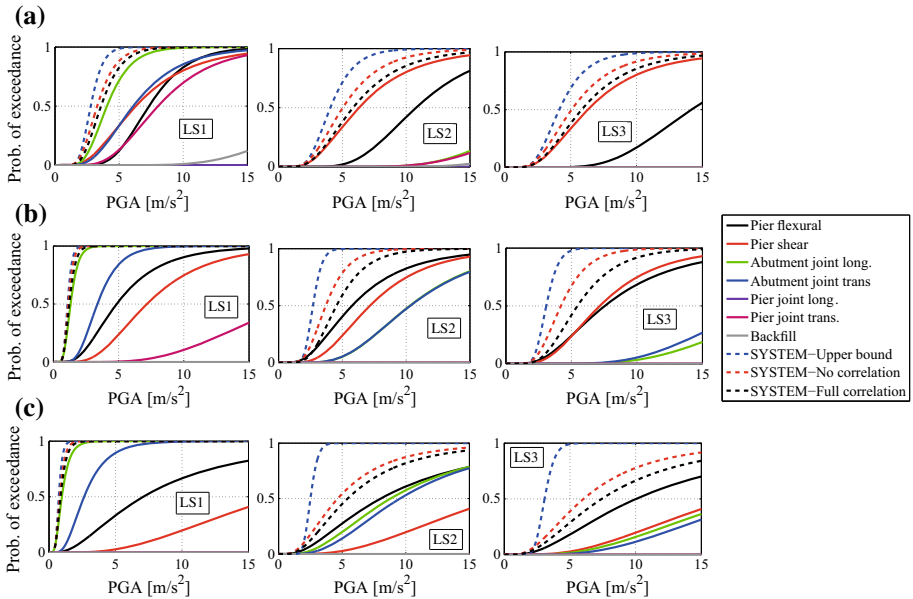

Fig. 13 Component and system fragility curves: **a** W08S2P02L15; **b** W14S3P05L30; **c** W20S4P08L30

piers is also probable. The deformations are under 1 cm in the design PGA range and lower than 5 cm at higher intensities, implying the low probability of superstructure unseating.

5.3 Derived fragility curves

General damage mechanisms are presented in Fig. 13 for two extreme cases (regarding the main structural parameters; W8S2P02L15 and W20S4P08L30) and for a typical highway

overpass bridge configuration (W14S3P05L30). It is highly possible that the abutment joint yields in the longitudinal direction and even transverse yielding of the abutment joint is expected to occur prior to the pier damage. The probability of backfill soil damage is nearly zero in the observed range of PGA. It can be concluded that the fragility of the system in LS1 is driven by the abutment joints. It is considered that after the joints yield, the bridge is still functional; LS2 is associated with the ultimate deformation capacity and full degradation of the joint rebars. The probability that the joints reach LS2 is lower. In case of bridges with short piers, there is a high probability that pier shear failure occurs before other components reach LS2; meaning that the bridge collapses with an unfavorable brittle failure mode right after the yielding of the system. If the pier height is increased, shear failure becomes less dominant; LS2 is characterized by pier flexural damage related to the spalling of concrete layers, and collapse is caused by the ductile flexural failure of the piers. It can also be observed that after the failure of the shear reinforcements of the joint in LS2, frictional forces still develop sufficiently preventing the superstructure from unseating (see the low probabilities related to joint deformations in LS3).

The results for the whole system in Fig. 13 indicate that the simple boundaries of the system fragility curves (blue dashed line for the upper bound and the most vulnerable component fragility curve for the lower bound) are relatively close to each other if one component dominantly governs the failure (see LS1 in Fig. 13b, for instance). As expected, system fragilities derived with the MC simulation fall in between the estimated simple boundaries. Considering no correlation between the component capacities results in higher probabilities compared to the full correlation estimation.

In Fig. 14a, system fragility curves are compared for different deck widths. It is observed that the component fragilities are higher for wider bridges which stems from the different seismic behavior in the transverse direction. The wider and stiffer the superstructure in the transverse direction, the more efficiently it can distribute the lateral forces to the stiff abutments. Accordingly, the probability of exceedance related to pier failure
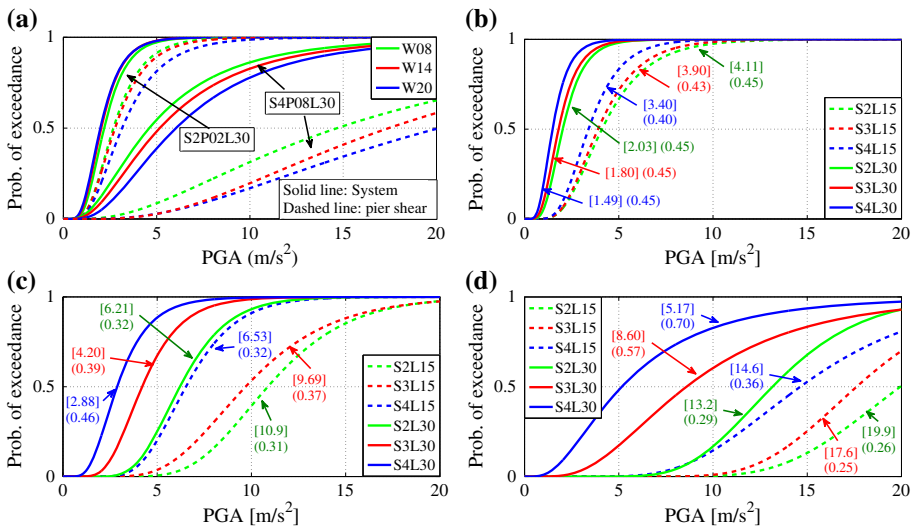

Fig. 14 System fragility curves for collapse (no correlation in capacity). **a** Comparison of different widths. **b** W14P02, **c** W14P05 and **d** W14P08 bridges. The median and LNSTD are in [] and () brackets, respectively

(shear or flexural) is higher if the deck width is smaller (note the component fragility curves for shear failure). If the component fragilities are relatively close to each other for different widths, the system fragility may be worse for wider bridges with more piers (see the S2P02L30 configuration in Fig. 14a), since the probability of failure increases with the number of possibly critical components if a series system is considered (i.e. all P_i component probabilities of each pier are taken into account in the MC simulation).

Figure 14b–d shows the system fragility curves of all W14 bridges. Although the bridges represent the same bridge class, significant difference can be observed for different layouts. Median values range between 1.5 and 20 m/s^2 and the LNSTD of the fragility curve is typically 0.25–0.45. Figure 14 also confirms that pier height significantly, while the span length moderately affect the fragility of the structure. It is apparent that the deck width is a less important structural attribute in case of PMG bridges.

5.4 Reliability of the structures

The β reliability index for a 50 year reference period of life service is determined for each configuration using Eqs. (6) and (7) and the hazard curves for Komárom and Debrecen (see Fig. 8b). The results are presented in Fig. 15 and Table 5, where the most vulnerable components are also indicated to show the weakest element of the system. The target reliability index a bridge should attain is not unique and varies from code to code. EC0 specifies target value only for Ultimate LS and Serviceability LS as 3.8 and 1.5, respectively for structures with moderate consequences of failure (RC2 class). In the Joint Committee on Structural Safety Model Code (JCSS 2001) it is proposed that the relative cost of safety measure (RCSM) should also be taken into account when selecting the target reliability index. It is stated that due to the large uncertainty in seismic loads a lower reliability class should be used. A β value of 1.98, 3.21 and 3.46 are proposed for large, normal and small RCSM, respectively, thus a 1.98 target reliability is adopted here to highlight structures that possibly need strengthening and retrofit.

The reliability index is decreasing with the length of the bridge (with the span length and the number of spans) and it is lower in case of short piers (e.g. the ranges of β values in the Debrecen area are 2.7–1.7, 3.6–2.2 and 4.3–2.4 for 2, 5 and 8 m pier heights, respectively). The first damage possibly occurs at the abutment joint, while the weakest component in LS2 depends on the actual layout. For short piers, shear failure is dominant meaning that the bridge collapses before other components could reach LS3. At higher piers, LS2 is reached at the abutment joint or at the pier (flexural damage indicated by the spalling of concrete) for shorter or longer spans, respectively. In most cases, the collapse is caused by the shear failure of the piers, however in case of more flexible configurations (with higher piers and longer spans) it is possible that pier flexural failure is dominant. The reliability indices for different deck widths show little difference, and the results are in
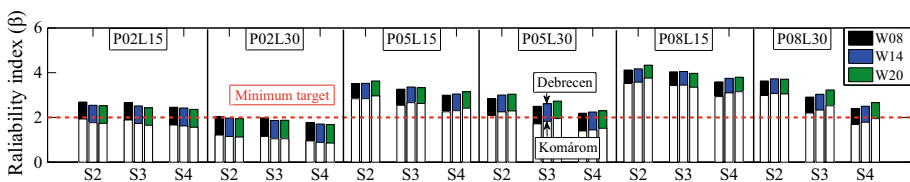

Fig. 15 Reliability indices (β) for collapse (no correlation in capacity) for two typical moderate seismic areas

Table 5 Weakest components (AJL—abutment joint longitudinal direction; SH—pier shear failure; FL—pier flexural failure) for LS1, LS2 and LS3; and reliability indices (β) related to collapse of W14 bridges for Komárom (FC—full correlation in capacity; NC—no correlation in capacity)

Configuration		Weakest component			β (collapse)		Configuration		Weakest component			β (collapse)	
		LS1	LS2	LS3	NC	FC			LS1	LS2	LS3	NC	FC
P02L15	S2	AJL	SH	SH	1.76	1.96	P05L30	S2	AJL	FL	SH	2.23	2.40
	S3	AJL	SH	SH	1.73	2.02		S3	AJL	FL	FL	1.80	2.03
	S4	AJL	SH	SH	1.63	1.91		S4	AJL	FL	FL	1.42	1.58
P02L30	S2	AJL	SH	SH	1.17	1.36	P08L15	S2	AJL	AJL	SH	3.55	3.78
	S3	AJL	SH	SH	1.04	1.35		S3	AJL	FL	FL	3.40	3.63
	S4	AJL	SH	SH	0.89	1.10		S4	AJL	AJL	FL	3.06	3.35
P05L15	S2	AJL	SH	SH	2.83	2.97	P08L30	S2	AJL	AJL	FL	3.02	3.27
	S3	AJL	SH	SH	2.68	2.94		S3	AJL	FL	FL	2.30	2.46
	S4	AJL	SH	SH	2.31	2.53		S4	AJL	FL	FL	1.73	1.82

accordance with the ones presented in Fig. 14a. Figure 15 shows that the reliability index is highly dependent on the considered design site. The difference in the reliability index is 0.55–0.85; e.g. the β of a typical highway overpass configuration (W14S3P05L30) is ~ 1.8 and ~ 2.6 if it is built in Komárom and Debrecen, respectively. Note that the bridge configuration is fixed (e.g. reinforcements, cross sections, capacities etc.), thus the results illustrate possible reliability indices of non-seismically designed bridges.

By comparing the computed reliability indices with the minimum target reliability index values, critical bridge configurations and design situations are characterized. Recognizing the tendencies in the reliability indices, with respect to the seismic vulnerability, bridges can be categorized on the basis of the pier height: *Group 1)* bridges with short piers (P02) and *Group 2)* bridges with normal or relatively high piers (P05 and P08). The collapse of bridges in *Group 1)* is characterized by pier shear failure, while bridges in *Group 2)* collapse with pier flexural failure. *Group 1)* is definitely more vulnerable and also less favorable due to the brittle failure mode. If these bridges are built in the Komárom area, all configurations could be considered as critical, while in case of the Debrecen area, the bridges are critical only over ~ 60 m total length. The bridges in *Group 2)* behave better, the reliability index is always over the minimum target value in the Debrecen area, while only bridges with a total length over 90–100 m are critical in the higher seismic area of Komárom.

6 Conclusions

The lack of seismic provisions in the pre-Eurocode ages questions the seismic performance of highway bridges in moderate seismic zones. Integral precast multi-girder bridges are popular in many moderately seismic European countries, such as in Hungary, where they have significant contribution to the whole bridge inventory both with their number and their estimated gross value. Their seismic performance that would be essential to estimate the economic consequences in case of a considerable earthquake is not known. Advanced and detailed modeling approach is used to carry out non-linear time-history analyses using hazard consistent ground motions. Due to the importance of the cyclic behavior of the

joints, a new modeling technique is worked out based on material model calibration using laboratory test data available in literature. A parametric seismic fragility analysis is conducted to examine the seismic behavior, to determine possible critical components and layouts associated with different damage limit states; and to estimate the probability of collapse of the whole structure. On the basis of the presented results, the following conclusions can be drawn:

- Modal analysis confirms that these structures are relatively stiff, the fundamental period often falls within the range of the constant plateau of the applied response spectrum.
- Investigation of the modeling assumptions shows that: (1) the monolithic joint behavior has a significant effect on the seismic demands; (2) omitting the participating mass of the embankment results in underestimated demands for shorter bridges; (3) using a bi-linear approximation for the backfill soil behavior generally leads to more conservative results; (4) the effect of the approaching slab and the wing walls are not significant and even negligible for longer bridges.
- It is shown that the usually applied power law for the Probabilistic Seismic Demand Model regression does not represent well certain component demands with large plastic deformations (e.g. reinforcing steel deformations).
- Evaluation of the appropriateness of various intensity measures shows that peak ground acceleration, acceleration spectrum intensity and Arias intensity describe well the expected demands for the entire range of the studied bridges.
- The fragility analysis concludes that it is highly possible that the first damage occurs at the abutment joints. After the joint yields, the governing damage in LS2 depends on the actual layout. Longer, more flexible bridges suffer pier flexural damage and full degradation of the shear reinforcements at the abutment joint may also occur. The collapse is caused by pier shear failure except for less rigid bridges (with more spans and high piers) in case of which pier flexural failure is more probable.
- The calculated reliability indices show that long bridges with short piers are highly susceptible to pier shear failure, these configurations should be retrofitted to reach at least the minimum target reliability.
- Since these bridges are not designed for seismic actions, the probability of collapse is highly dependent on the actual design site. A difference in the reliability index of 0.55–0.85 is observed considering two typical moderate seismic areas.
- The study illustrates that the probability of collapse of integral precast multi-girder bridges may be high (the β index for a 50 year reference period may fall below 1) even in moderate seismic regions due to the lack of seismic design and insufficient seismic detailing.

The presented results are directly applicable for the modeling, analysis and design of integral precast multi-girder bridge systems in moderate seismic zones.

References

Akiyama H, Kajikawa Y (2008) Fundamentally structural characteristics of integral bridges. Thesis, Graduate School of Natural Science and Technology Kanazawa University

Akkar S, Bommer JJ (2010) Empirical equations for the prediction of PGA, PGV and spectral accelerations in Europe, the Mediterranean Region and the Middle East. Seismol Res Lett 81(2):195–206. doi:10.1785/gssrl.81.2.195

Avşar Ö, Yakut A, Caner A (2011) Analytical fragility curves for ordinary highway bridges in Turkey. Earthq Spectra 27(4):971–996. doi:10.1193/1.3651349

Baker JW (2011) Conditional mean spectrum: tool for ground motion selection. J Struct Eng 137(3):322–331. doi:10.1061/(ASCE)ST.1943-541X.0000215

Baker JW (2015) Efficient analytical fragility function fitting using dynamic structural analysis. Earthq Spectra 31(1):579–599. doi:10.1193/021113EQS025M

Basoz N, Kiremidjian AS (1996) Risk assessment for highway transportation systems. Report No. NCEER-118, John A. Blume Earthquake Engineering Center

Biskinis D, Roupakias G, Fardis MN (2004) Degradation of shear strength of RC members with inelastic cyclic displacements. ACI Struct J 101(6):773–783

Borzi B, Ceresa P, Franchin P, Noto F, Calvi GM, Pinto PE (2015) Seismic vulnerability of the Italian roadway bridge stock. Earthq Spectra 31(4):2137–2161. doi:10.1193/070413EQS190M

Bradley BA (2010) A generalized conditional intensity measure approach and holistic ground-motion selection. Earthq Eng Struct Dyn 39(12):1321–1342. doi:10.1002/eqe.995

Bradley BA (2012a) The seismic demand hazard and importance of the conditioning intensity measure. Earthq Eng Struct Dyn 41(11):1417–1437. doi:10.1002/eqe.2221

Bradley BA (2012b) A ground motion selection algorithm based on the generalized conditional intensity measure approach. Soil Dyn Earthq Eng 40(1):48–61. doi:10.1016/j.soildyn.2012.04.007

Caltrans (2013) Caltrans seismic design criteria. California Department of Transportation, Sacramento, CA, Version 1.7

CEN (2008a) MSZ EN 1998-1 Eurocode 8: design of structures for earthquake resistance. Part 1: general rules, seismic actions and rules for buildings

CEN (2008b) MSZ EN 1998-1 Eurocode 8: design of structures for earthquake resistance. Part 2: bridges

CEN (2009) MSZ EN 1998-5 Eurocode 8: design of structures for earthquake resistance. Part 5: foundations, retaining structures and geotechnical aspects

CEN (2011a) MSZ EN 1998-3 Eurocode 8: design of structures for earthquake resistance. Part 3: assessment and retrofitting of buildings

CEN (2011b) MSZ EN 1990-1 Eurocode 0: basis of structural design

Charney FA (2008) Unintended consequences of modeling damping in structures. J Struct Eng 134(4):581–592. doi:10.1061/(ASCE)0733-9445(2008)134:4(581)

Connal J (2004) Integral abutment bridges-Australian and US practice. 5th Austroads bridge conference, Hobart, Tasmania

Elnashai AS, Di Sarno L (2008) Fundamentals of earthquake engineering. Wiley, UK

England GL, Tsang NCM, Bush DI (2000) Integral bridges: a fundamental approach to the time-temperature loading problem. Thomas Telford, London

Fennema J, Laman J, Linzell D (2005) Predicted and measured response of an integral abutment bridge. J Bridge Eng 10(6):666–677. doi:10.1061/(ASCE)1084-0702(2005)10:6(666)

FIB (2008) Bulletin 43: Structural connections for precast concrete buildings. International Federation for Structural Concrete

Franchin P, Pinto PE (2014) Performance-based seismic design of integral abutment bridges. Bull Earthq Eng 12(2):939–960. doi:10.1007/s10518-013-9552-2

Goldberg DE (1989) Genetic algorithm in search, optimization, and machine learning. Kluwer Academic Publishers, Boston

HTA (2015) Integrated bridge database. Hungarian Transport Administration

Jalayer F, Cornell CA (2009) Alternative nonlinear demand estimation methods for probability-based seismic assessments. Earthq Eng Struct Dyn 38(8):951–972. doi:10.1002/eqe.876

JCSS (2001) Probabilistic model code. Joint Committee on Structural Safety, Zurich. ISBN 978-3-909386-79-6

Kappos A, Sextos AG (2009) Seismic assessment of bridges accounting for nonlinear material and soil response, and varying boundary conditions. Part of the series NATO Science for Peace and Security Series C: Environmental Security pp 195–208

Kaufmann W (2011) Swiss federal roads office guidelines for integral bridges. Struct Eng Int 21(2):189–194

Kibboua A, Bechtoula H, Mehani Y, Naili M (2014) Vulnerability assessment of reinforced concrete bridge structures in Algiers using scenario earthquakes. Bull Earthq Eng 12(2):807–827. doi:10.1007/s10518-013-9523-7

Maroney BH (1995) Large scale bridge abutment tests to determine stiffness and ultimate strength under seismic loading. PhD thesis, Dept. of Civil Engineering, University of California Davis, CA

McKenna F, Scott MH, Fenves GL (2010) Nonlinear finite-element analysis software architecture using object composition. J Comput Civil Eng 24(1):97–105. doi:10.1061/(ASCE)CP.1943-5487.0000002

Mitoulis SA (2012) Seismic design of bridges with the participation of seat-type abutments. Eng Struct 44(1):222–233. doi:10.1016/j.engstruct.2012.05.033

Moschonas IF, Kappos AJ, Panetsos P, Papadopoulos V, Makarios T, Thanopoulos P (2009) Seismic fragility curves for Greek bridges: methodology and case studies. Bull Earthq Eng 7(2):439–468. doi:10.1007/s10518-008-9077-2

Nakamura S, Momijama Y, Hosaka T, Homma K (2002) New technologies of steel/concrete composite bridges. J Constr Steel Res 58(1):99–130. doi:10.1016/S0143-974X(01)00030-X

Nielson BG (2005) Analytical fragility curves for highway bridges in moderate seismic zones. PhD dissertation, School of Civil and Environmental Engineering, Georgia Institute of Technology

Nowak AS, Collins KR (2000) Reliability of structures. The McGraw-Hill Companies Inc, USA

Padgett JE (2007) Seismic vulnerability assessment of retrofitted bridges using probabilistic methods, PhD Dissertation, 2007, School of Civil and Environmental Engineering—Georgia Institute of Technology

PEER (2015) NGA-West2 database: shallow crustal earthquakes in active tectonic regimes. Pacific Earthquake Engineering Research Center, University of California, Berkeley

Priestley MJN, Seible F, Calvi GM (1996) Seismic design and retrofit of bridges. Wiley, New York

Psycharis NI, Mouzakis PH (2012) Shear resistance of pinned connections of precast members to monotonic and cyclic loading. Eng Struct 41(1):413–427. doi:10.1016/j.engstruct.2012.03.051

Sextos AG, Taskari O (2008) Comparative assessment of advanced computational tools for embankment-abutment-bridge superstructure interaction. The 14th World Conference on Earthq Eng, Beijing, China

Shamsabadi A, Rollins K, Kapuskar M (2007) Nonlinear soil–abutment–bridge structure interaction for seismic performance-based design. J Geotech Geoenviron 133(6):707–720. doi:10.1061/(ASCE)1090-0241(2007)133:6(707)

Simon J, Vigh LG (2015) Preliminary seismic vulnerability assessment of pre-code multi-girder bridges in Hungary, SECED Conference: Earthq Risk and Eng towards a Resilient World. Cambridge, UK, pp 1–10

Simon J, Vigh LG, Horváth A, Pusztai P (2015) Application and assessment of equivalent linear analysis method for conceptual seismic retrofit design of Háros M0 highway bridge. Period Polytech 59(2):109–122. doi:10.3311/PPci.7860

Solomos G, Pinto A, Dimova S (2008) A review of the seismic hazard zonation in national building codes in the context of Eurocode 8. JRC Scientific and Technical Reports

Tóth L, Győri E, Mónus P, Zsíros T (2006) Seismic hazard in the Pannonian region. The Adria Microplate: GPS Geodesy, Tectonics, and Hazards, Springer Verlag, NATO ARW Series 61(1):369–384. doi: 10.1007/1-4020-4235-3_25

ÚT (2004) Útügyi Műszaki Előírás ÚT 2-3.401 Közúti hidak tervezése, Általános előírások. Magyar Útügyi Társaság (in Hungarian)

Vamvatsikos D, Cornell CA (2002) Incremental dynamic analysis. Earthq Eng Struct Dyn 31(3):491–514. doi:10.1002/eqe.141

Vigh LG, Dunai L, Kollár L (2006) Numerical and design considerations of earthquake resistant design of two Danube bridges. 1st European Conference on Earthq Eng and Seism, Switzerland, Paper 1420

Wasserman EP (2007) Integral abutment design (practices in the United States). First US-Italy seismic bridge workshop, Pavia

White H, Pétursson H, Collin P (2010) Integral abutment bridges: the European Way. Pract Period Struct Des Constr 15(3):201–208. doi:10.1061/(ASCE)SC.1943-5576.0000053

Wolf JP (1985) Dynamic soil-structure interaction. Prentice-Hall Inc, New Jersey

Zhang J, Makris N (2002) Kinematic response functions and dynamic stiffnesses of bridge embankments. Earthq Eng Struct Dyn 31:1933–1966. doi:10.1002/eqe.196

Zsarnóczay Á, Vigh LG, Kollár L (2014) Seismic performance of conventional girder bridges in moderate seismic regions. J Bridge Eng 19(5): 9. Paper 04014001. doi: 10.1061/(ASCE)BE.1943-5592.0000536